

Large reversible magnetocaloric effect of the EuAl₃Si single crystal

Hai Zeng*, Shuo Zou, Zhou Wang, Ziyu Li, Kangjian Luo and Yongkang Luo*

Wuhan National High Magnetic Field Center and School of Physics,

Huazhong University of Science and Technology, Wuhan 430074, China

Abstract

The magnetic properties, magnetocaloric effect and magnetoresistance of EuAl₃Si single crystal have been investigated. A giant reversible magnetocaloric effect was observed around $T_C = 14.5$ K. For the low magnetic field changes of 0-2 T, the maximum values of magnetic entropy change and refrigerant capacity are 13.4 J/kg K, and 166 J/kg, respectively, with the corresponding adiabatic temperature of 7.2 K. These excellent magnetocaloric parameters suggest EuAl₃Si as a promising candidate for magnetic refrigeration application around liquid hydrogen temperature.

Keywords: Ferromagnetic materials; EuAl₃Si; Magnetocaloric effect; Magnetic refrigeration

Corresponding authors:

* E-mail addresses: mpzsllyk@gmail.com (Yongkang Luo) and zenghai320@sina.com (Hai Zeng)

Magnetic refrigeration based on the magnetocaloric effect (MCE) has attracted much attention for the potential alternative approach to conventional gas-compression refrigeration due to its bigger refrigeration capacity and lower environmental influences.¹ The MCE refers to the phenomenon where a magnetic material absorbs or releases heat due to the change in magnetic entropy during magnetization or demagnetization. Adiabatic demagnetization, which employs this effect, is one of the mainstream methods for achieving milli-Kelvin ultralow temperatures.² Both isothermal magnetic entropy change (ΔS_M) and adiabatic temperature change (ΔT_{ad}) can characterize the MCE of materials. Many new magnetic materials with giant MCE have been widely studied for this purpose, especially for below the temperature region of liquid nitrogen.³⁻⁶ However, most of them are less efficient when designing magnetic refrigeration due to the large magnetic/thermal hysteresis and aging effect accompanied by the first-order magnetic transition or the coupling between the magnetic transition and structural transformation.⁷⁻⁹ Another important parameter to evaluate this property is refrigeration capacity (RC). Therefore, it is important to search for new magnetic-refrigeration materials with considerable MCE and RC in low magnetic fields (e.g., $\Delta H \leq 2T$) and wide temperature range for applications.

Rare-earth (RE)-based compounds have gathered much attention in recent years due to low field induced considerable MCE.¹⁰⁻¹⁶ Among them, Eu^{2+} ($4f^7$, $S = 7/2$), which can be regulated easily by magnetic field, pressure or temperature, are a good platform for studying various exotic phenomena including the magnetocaloric effect.¹⁵⁻

¹⁷ Recently, EuAl_4 is extensively investigated due to its rich and unique magnetic and

electronic behaviors such as three successive antiferro-magnetic transitions in charge-density-wave ordered state,¹⁸⁻²² possible topological Hall effect²³ and magnetic skyrmions.²⁴ Partial substitution of Al by Si yields EuAl₃Si that retains the crystal structure²⁵. However, little has been known about its physical properties.

In this paper, we report a detailed study on the magnetic properties, MCEs and transport properties of EuAl₃Si by magnetization, resistivity, and heat capacity measurements. The Eu moments order ferromagnetically below $T_C = 14.5$ K. The magnetic order can be easily controlled by applying a tiny magnetic field presented as a negative magnetoresistance. A giant low field reversible MCE was obtained around 20 K. The maximal values of $-\Delta S$ are 10 and 17 J/kg K for field changes of 0-2 T and 0-4 T, respectively. Our results suggest that EuAl₃Si is a promising material for magnetic refrigeration in the liquid-hydrogen temperature region.

EuAl₃Si single crystals were grown by the Al-flux method using the raw materials Eu (Energy Chemical, 99.9%), Al (Alfa Aesar, 99.9999%) and Si (Alfa Aesar, 99.9999%) in the molar ratio of Eu: Si: Al = 1:1:20. The mixture was loaded in an alumina crucible and subsequently sealed in an evacuated quartz tube. The latter was heated up to 1175 °C, dwelled for 24 h, and then slowly cooled down to 750 °C at a rate of 1 °C/h. The Al flux was removed by centrifugation at 750 °C. The obtained plate single crystal is typically about 3×1.5×0.8 mm³ and is stable in air as shown in the inset of Fig. 1(b).

The composition of the compound was confirmed by energy-dispersive X-ray spectroscopy (EDS). The crystal structure and crystallographic orientation was

determined by X-Ray diffraction (XRD) at room temperature. Rietveld refinements were carried out to obtain its structural information. Measurements of magnetization, electrical resistivity and specific heat were performed in a Physical Properties Measurements System (PPMS, Quantum Design). The isothermal magnetization curves with magnetic field applied along the c axis and ab plane were measured. Electrical resistance was measured by the standard four-probe method. To avoid spurious resistivity contributions, the resistivity curves of Hall resistivity ρ_{xy} and longitudinal electrical resistivity ρ_{xx} were respectively manipulated by a field symmetrization procedures: $\rho_{xx}(H) = [\rho_{xx}(H) + \rho_{xx}(-H)]/2$.

EuAl₃Si crystallizes in the BaAl₄-type centrosymmetric tetragonal structure ($I4/mmm$, No.139) as illustrated in Fig.1(a). The Eu atoms locate at the $2a$ (0, 0, 0) site and Al atoms occupy the $4d$ (0.5, 0, 0.25) site (Al1), while the rest of Al atoms (Al2) and Si atoms are randomly distributed in the $4e$ (0, 0, 0.3857) site. Figure 1(b) represents the EDS results for the sample, where the chemical proportions are determined as Eu : Al : Si = 1 : 3.02 : 1.04, approaching closely the nominal composition. Figure 1(c) shows the Rietveld refinement of the XRD pattern. No extraneous phases could be identified. The lattice parameters obtained are $a = b = 4.410(1)$ Å, $c = 10.918(5)$ Å, which is consistent with data reported previously.²⁵ The XRD diffraction pattern for c -axis, corresponding well to the (0 0 $2l$) plane as shown in Fig. 1(d). The high resolution x-ray curve shown in the inset gives the full-width at half-maximum (FWHM) $\theta = 0.042^\circ$, indicating the high quality of the single crystal.

Figure 2(a) shows the temperature dependence of magnetic susceptibility at μ_0H

= 0.1 T with the magnetic field parallel to the ab plane ($H//ab$ plane) and c axis ($H//c$ axis). At high temperature, both χ_{ab} and χ_c obey well to the Curie-Weiss law, $\chi = C_0 / (T - \theta_{cw})$, where C and θ_{cw} are the Curie constant and paramagnetic Curie temperature, respectively. To determine the effective moments (μ_{eff}) and θ_{cw} , the powder-averaged magnetic susceptibility is calculated, $\chi_{\text{avg}} = (\chi_c + 2\chi_{ab})/3$, the inverse of which is shown in the inset to Fig. 1(a) as a function of T . The Curie-Weiss fitting of $\chi_{\text{avg}}(T)$ leads to $\mu_{\text{eff}} = 7.99 \mu_B/\text{Eu}$, and $\theta_{cw} = 14.36$ K. The effective moment is close to the theoretical values for Eu^{2+} ($g\sqrt{S(S+1)}\mu_B = 7.94 \mu_B$, $S = 7/2$). The positive θ_{cw} confirms the FM correlation. At low temperature, χ_{ab} is significantly larger than χ_c , and the value increases rapidly before saturating in the $T \rightarrow 0$ limit, on the contrary, χ_c shows a small peaks near 14.5 K below which it tends to level off. Such a behavior indicates that the Eu moments undergo a FM transition near $T_C = 14.5$ K, and the moments align in the ab plane. The magnetization curves rapidly rise and reach saturation gradually below T_C in both directions at 2 K as shown in Fig. 3, showing a FM behavior. The saturated moment is $M_{\text{sat}} = 6.92 \mu_B$ per Eu^{2+} above 0.8 T at 2 K for $H//ab$ plane. A larger critical field $H_C \sim 2$ T is needed to saturate for the other direction. The large magnetization and low saturation magnetic field make it possible for a magnetocaloric materials to exhibit a giant reversible MCE. The FM transition is also visible in specific heat as shown in Fig. 2(c).

To explore the response of magnetism on magnetotransport, the electrical resistivity (ρ_{xx}) was measured. The $\rho_{xx}(T)$ presents a typical metallic behavior and a remarkably kink is observed at $T_C = 14.5$ K by reason of the magnetic ordering, as

shown in Fig. 2(d). The single crystal displays a residual resistivity of $\rho_0 = 6.19 \mu\Omega$ cm and a modest residual resistivity ratio (RRR) $\rho_{xx}(300 \text{ K})/\rho_{xx}(1.8 \text{ K}) \sim 1.5$. The $\rho_{xx}(T)$ curve can be well fitted on the data from 48 to 300 K using the Bloch-Grüneisen model:²⁶

$$\rho(T) = \rho_0 + C \left(\frac{T}{\Theta_D} \right)^5 \int_0^{\frac{\Theta_D}{T}} \frac{x^5}{(e^x - 1)(1 - e^{-x})} dx, \quad (1)$$

where ρ_0 is the residual resistivity and Θ_D is the Debye temperature. The refined $\Theta_D = 445 \text{ K}$, $C = 16.18 \mu\Omega \text{ cm}$. Fig. 2(e) shows the temperature dependence of longitudinal resistivity with the $H//c$ axis for field from 0 to 8 T. As the magnetic field increases, the kink at T_C shifts to lower temperature and gradually fades away as the magnetic moments are aligned under the magnetic field. As seen in Fig. 2(f), the negative magnetoresistances are observed both for $H//ab$ and $H//c$ at 1.8 K. The inflection points in $\rho_{xx}(H)$ signify the field-induced polarization of Eu moments, and the values are 0.8 T and 2.0 T for $H//ab$ and $H//c$, respectively; both are consistent with magnetization isotherms.

To investigate the MCE in EuAl₃Si single crystal, the isothermal magnetization curves have been measured with the field along the crystallographic directions from 2 to 60 K, as shown in Fig. 3(a) and (b). For $H//ab$ and $H//c$, the magnetization increases with the magnetic field, as shown in Fig. 2(b). With the temperature rising, the magnetization decreases gradually and H_C moves to a higher value below T_C . Magnetic hysteresis is nearly unobservable in both directions around 15 K, which again implies a second-order phase transition.

The magnetic entropy change $[\Delta S_M(T, H)]$ of EuAl₃Si was calculated based on

the isothermal magnetization around T_C by the Maxwell's relation:⁷

$$\Delta S_M(T, H) = S_M(T, H) - S_M(T, 0) = \int_0^H \left[\frac{\partial M(H, T)}{\partial T} \right]_H dH. \quad (2)$$

The temperature dependences of $-\Delta S_M(T)$ for different magnetic field variations ΔH are shown in Fig. 3(a) and (b). Each curves shows a peak near 15 K, revealing the giant MCE originates from the sharp change of magnetization near FM transition. The maximum values of $-\Delta S_M(T)$ reach 13.4 J/kg K and 10.4 J/kg K for the relatively small magnetic field change $\Delta H = 2$ T with field along with ab plane and c axis, respectively. The RC is another important quality factor to evaluate the MCE. The RC is calculated by using the equation:

$$RC = \int_{T_1}^{T_2} | \Delta S_M | dT, \quad (3)$$

where T_1 and T_2 are the boundary value of the full width at half maximum in $-\Delta S_M(T)$ curve, respectively. Fig. 3(c) shows the field dependence RC in both directions. Apparently, the RC values increase monotonically with magnetic field. For a field change of 0-2 T, the value of RC is 166 J/kg and 92 J/kg with $H//ab$ plane and $H//c$ axis, respectively. A third important parameter of magnetic refrigerant materials is the adiabatic temperature change ΔT_{ad} , which is obtained from the $C(T)$ data by:

$$\Delta T_{ad}(T, H) = -\Delta S_M(T, H) \frac{T}{C_p}, \quad (4)$$

where C_p is zero-field specific heat as shown in Fig. 2(b). The field dependences of ΔT_{ad} for EuAl_3Si with $H//ab$ plane and c axis at 19 K is shown in Fig. 3(d). For field changes of 2 T, the values of ΔT_{ad} are estimated to be 7.2 K and 5.5 K, respectively. Around the liquid hydrogen temperature (about 20 K), EuAl_3Si exhibits considerable $-\Delta S_M(T)$, RC and ΔT_{ad} for the relative low magnetic field changes of 0-2 T, suggesting

that EuAl_3Si is a promising material in hydrogen liquefaction. For a comparison, the effective parameters of MCE under the field change of 0-2 T for EuAl_3Si and some other typical magnetic refrigeration materials with similar magnetic transition temperature T_M are listed in Table I. It can be seen that the MCE parameters of EuAl_3Si are comparable or even larger than those of the reference substances. There has been a significant MCE performance enhancement compared to EuAl_4 . Therefore, EuAl_3Si could be an attractive candidate for the magnetic refrigeration working around liquid-hydrogen temperature under low magnetic field change.

In summary, a systematic investigation of magnetic, magnetotransport, and magnetocaloric properties of EuAl_3Si have been carried out. A giant reversible MCE and large RC have been observed around 15 K. With the relative low magnetic field changes of 0-2 T, the maximum value of $-\Delta S_M$, RC and ΔT_{ad} reach 13.4 J/kg K, 166 J/kg, and 7.2 K, respectively, which are comparable if not larger than other refrigeration materials around liquid hydrogen temperature. The excellent magnetocaloric properties indicate that EuAl_3Si can be a promising candidate to the liquefaction of hydrogen gas.

This work is supported by the National Key R&D Program of China (2022YFA1602602, 2023YFA1609600), Fundamental Research Funds for the Central Universities (YCJJ20230108), National Natural Science Foundation of China (U23A20580), the open research fund of Songshan Lake Materials Laboratory (2022SLABFN27), and Guangdong Basic and Applied Basic Research Foundation

(2022B1515120020).

The data that support the findings of this study are available from the corresponding authors upon reasonable request.

REFERENCES

¹V. Franco, J. S. Blázquez, J. J. Ipus, J. Y. Law, L. M. Moreno-Ramírez, and A. Conde, [Prog. Mater Sci. **93**, 112-232 \(2018\)](#).

²W. Giauque, and D. P. MacDougall, [Phys. Rev. **43**, 768-768 \(1933\)](#).

³J. Chen, B. G. Shen, Q. Y. Dong, and J. R. Sun, [Appl. Phys. Lett. **95**, 132504 \(2009\)](#).

⁴Z.-J. Mo, J. Shen, L.-Q. Yan, and C.-C. Tang, [Appl. Phys. Lett. **103**, 052409 \(2013\)](#).

⁵X. Q. Zheng, X. P. Shao, J. Chen, Z. Y. Xu, F. X. Hu, J. R. Sun, and B. G. Shen, [Appl. Phys. Lett. **102**, 022421 \(2013\)](#).

⁶L. Li, Y. Yuan, Y. Zhang, T. Namiki, K. Nishimura, and R. P€ottgen, [Appl. Phys. Lett. **107**, 132401 \(2015\)](#).

⁷V. K. Pecharsky, and K. A. Gschneidner, [Phys. Rev. Lett. **78**, 4494 \(1997\)](#).

⁸F. Hu, B. Shen, J. Sun, Z. Cheng, G. Rao, and X. Zhang, [Appl. Phys. Lett. **78**, 3675-3677 \(2001\)](#).

⁹F. Hu, B. Shen, J. Sun, and G. Wu, [Phys. Rev. B **64**, 132412 \(2001\)](#).

¹⁰Z. Mo, J. Shen, L.-Q. Yan, J.-F. Wu, and B.-G. Shen, [Appl. Phys. Lett. **102**, 192407 \(2013\)](#).

¹¹L. Li, O. Niehaus, M. Kersting, and R. P€ottgen, [Appl. Phys. Lett. **104**, 092416 \(2014\)](#).

- ¹²L. M. da Silva, A. O. dos Santos, A. A. Coelho, and L. P. Cardoso, [Appl. Phys. Lett.](#) **103**, 1622413 (2013).
- ¹³X. Zhao, X. Zheng, X. Luo, F. Gao, and S. C. Ma, [J. Mater. Sci. Technol.](#) **86**, 56-63 (2021).
- ¹⁴Y. Yuan, Y. Wu, X. Tong, H. Zhang, H. Wang, X. J. Liu, L. Ma, H. L. Suo, and Z.P. Lu, [Acta Mater.](#) **125**, 481-489 (2017).
- ¹⁵S. Wang, Q. Luo, X. Luo, S. C. Ma, and C. C. Chen, [J. Alloys Compd.](#) **968**, 171977 (2023).
- ¹⁶H. Xie, W. Su, H. Lu, Z. Mo, D. Wang, H. Sun, L. Tian, and J. Shen, [J Mater. Sci. Technol.](#) **118**, 128-135 (2022).
- ¹⁷S. Klenner, Z. Zhang, R. Pottgen, and L. Li, [Intermetallics](#), **120**, 106765 (2020).
- ¹⁸A. Nakamura, T. Uejo, F. Honda, T. Takeuchi, and H. Harima, [J. Phys. Soc. Jpn.](#) **84**, 124711 (2015).
- ¹⁹S. Araki, Y. Ikeda, T. C. Kobayashi, A. Nakamura, and Y. Hiranaka, [J. Phys. Soc. Jpn.](#) **83**, 015001 (2014).
- ²⁰A. Nakamura, Y. Hiranaka, and M. Hedo, [JPS Conf. Proc.](#) **3**, 011012 (2014).
- ²¹S. Shimomura, H. Murao, S. Tsutsui, H. Nakao, A. Nakamura, M. Hedo, T. Nakama, and Y. Ōnuki, [J. Phys. Soc. Jpn.](#) **88**, 014602 (2019).
- ²²M. Kobata, S. Fujimori, Y. Takeda, and T. Okane, [J. Phys. Soc. Jpn.](#) **85**, 094703 (2016).
- ²³T. Shang, Y. Xu, D. J. Gawryluk, J. Z. Ma, T. Shiroka, M. Shi, and E. Pomjakushina, [Phys. Rev. B](#) **103**, L020405 (2021).
- ²⁴Rina Takagi, N. Matsuyama, V. Ukleev, L. Yu, and J. S. White, [Nat. Commun.](#) **13**,

[1472 \(2022\)](#).

²⁵P. H. Tobash, and S. Bobev, [J. Alloys Compd. **418**, 58-62 \(2006\)](#).

²⁶M. Ziman, Clarendon Press: [Oxford, U.K., 1962](#).

²⁷L. Meng, C. Xu, Y. Yuan, Y. Qi, S. Zhou, and L. Li, [RSC Adv., **6**, 74765 \(2016\)](#).

²⁸Q. Y. Dong, J. Chen, J. Shen, J. R. Sun, and B. G. Shen, [Appl. Phys. Lett. **99**, 132504 \(2011\)](#).

²⁹H. Zhang, B. G. Shen, Z. Y. Xu, J. Shen, F. X. Hu, J. R. Sun, and Y. Long, [Appl. Phys. Lett. **102**, 092401 \(2013\)](#).

³⁰P. J. von Ranke, V. K. Pecharsky, and K. A. Gschneidner, [Phys. Rev. B **58**, 110-116 \(1998\)](#).

Figure captions

FIG. 1 (a) Schematic diagram of the crystal structure of EuAl_3Si ; red, cinerous, and blue balls represent Eu, Al, and Si atoms, respectively. (b) EDS for the crystal. (c) Observed and refined XRD patterns of EuAl_3Si ; inset shows the photograph of a representative single crystal on millimeter-grid paper. (d) The XRD pattern of the crystal plane of $(0\ 0\ 2l)$; inset gives the high resolution x-ray curve.

FIG. 2 (a) Zero-field-cooling (ZFC) and Field-cooling (FC) measurements of the magnetization under fields of 0.1 T with $H//ab$ plane and $H//c$ axis; inset shows the corresponding inverse susceptibility χ^{-1} . (b) Magnetization curves measured at 2 K. (c) The temperature dependence of specific heat of EuAl_3Si single crystal. (d) The temperature dependence of resistivity of EuAl_3Si single crystal. The red line represents the fitting using the Bloch-Gruneisen model. (e) resistivity as a function of temperature under different magnetic fields parallel to the c axis. (f) Magnetic field dependence of the resistivity at 1.8K with the field along the ab plane and c axis.

FIG. 3 Isothermal magnetization curves along ab plane (a) and c axis (b), respectively.

FIG. 4 The temperature dependence of $-\Delta S_M$ along the ab plane (a) and c axis (b) under various field changes. The magnetic field dependence of RC (c) and ΔT_{ad} at 19 K (d) along the ab plane and c axis.

Table I

The magnetic transition temperature (T_M), $-\Delta S_M$, RC , and ΔT_{ad} with the field changes of 0-2 T for EuAl_3Si , and some other typical magnetic refrigeration materials around the liquid hydrogen temperature. The symbol “-” represents the value was not reported in the literatures.

Material	T_M (K)	$-\Delta S_M$ (J/kg K), 2T	RC (J/kg), 2T	ΔT_{ad} (K), 2T	Reference
EuAl_3Si	14.5	13.4	166	7.2	this work
EuAl_4	15.8	8.4	67	-	15
GdCoC_2	15	16	160	-	27
Er_3Ni_2	17	11	-	3.3	28
TmGa	11.5/15	20.6	149	5	4
ErFeSi	22	14.2	130	3.4	29
DyNi_2	20	10.7	-	4.2	30
TmZn	8	19.6	-	3.3	6

FIG. 1

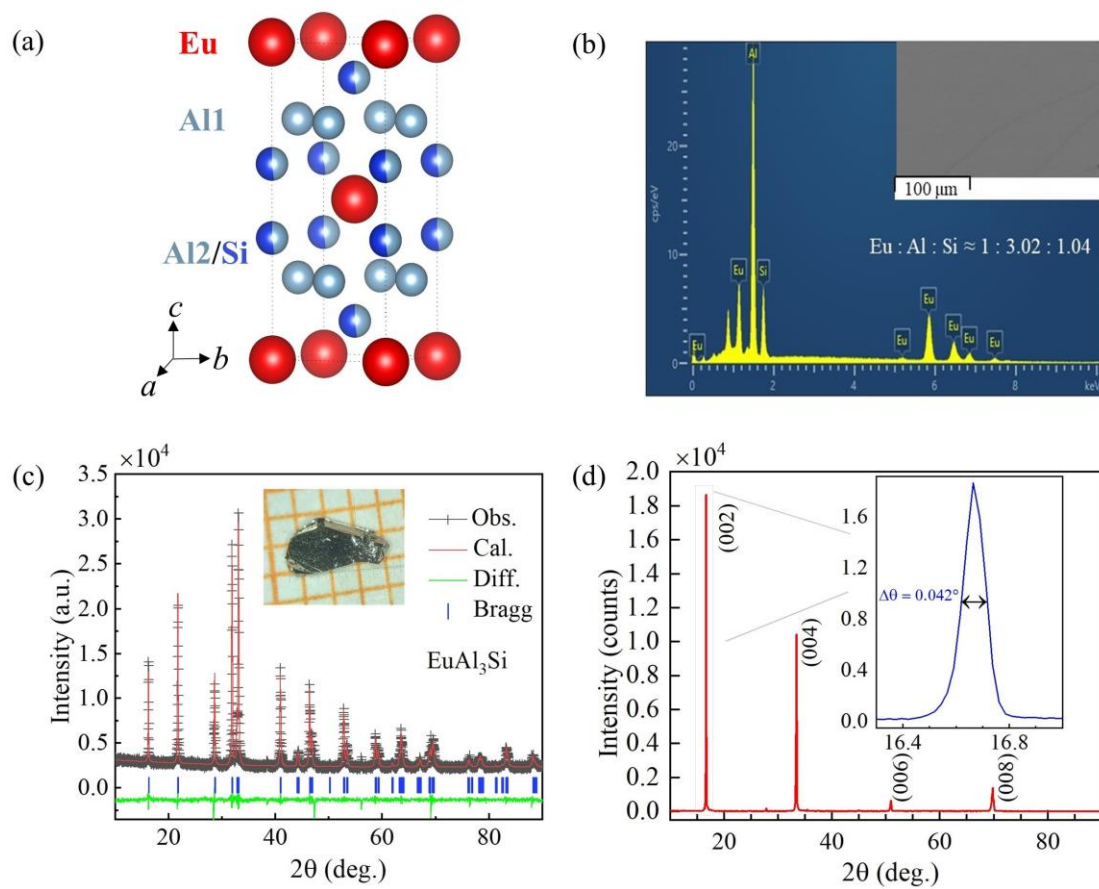


FIG. 2

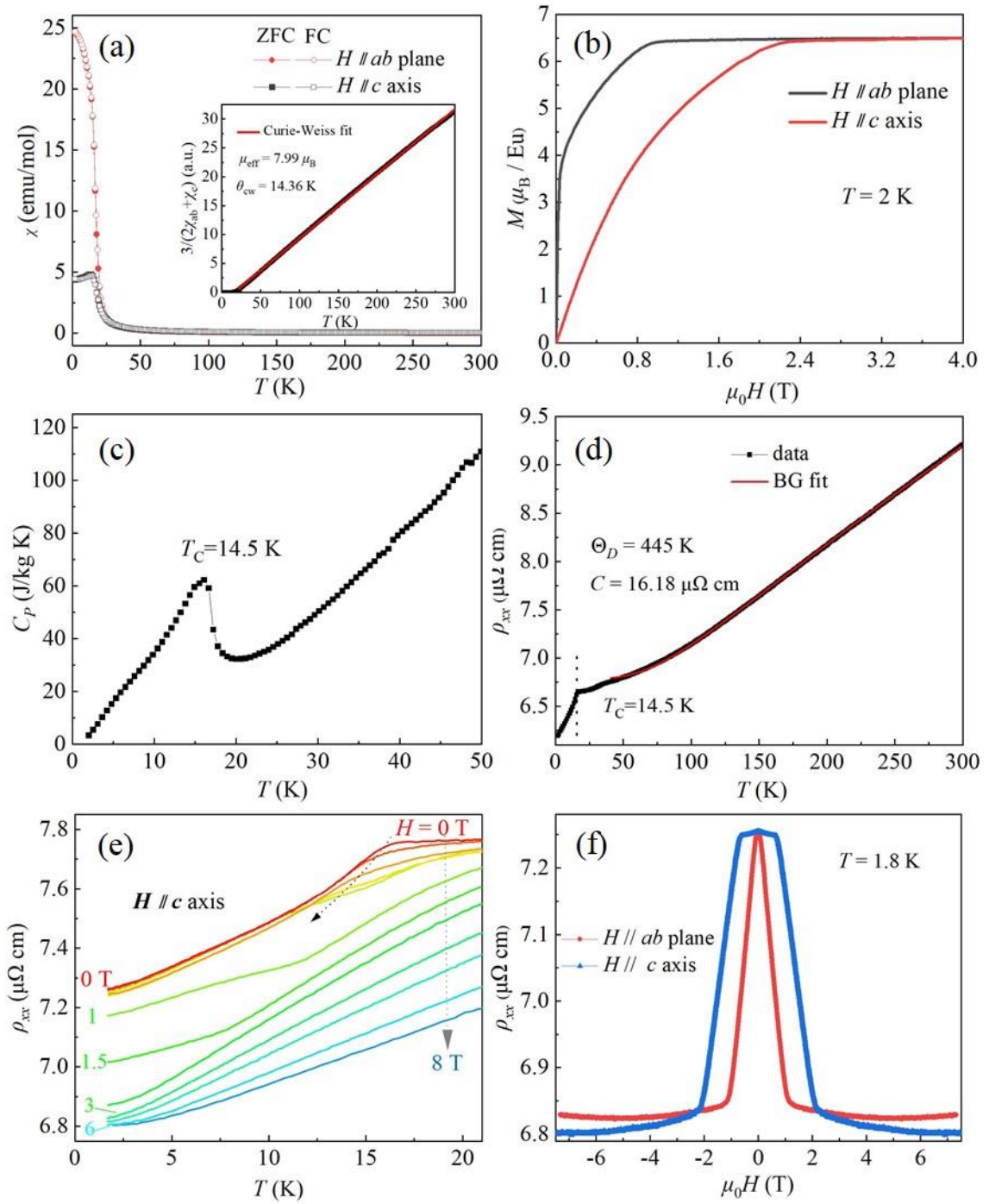


FIG. 3

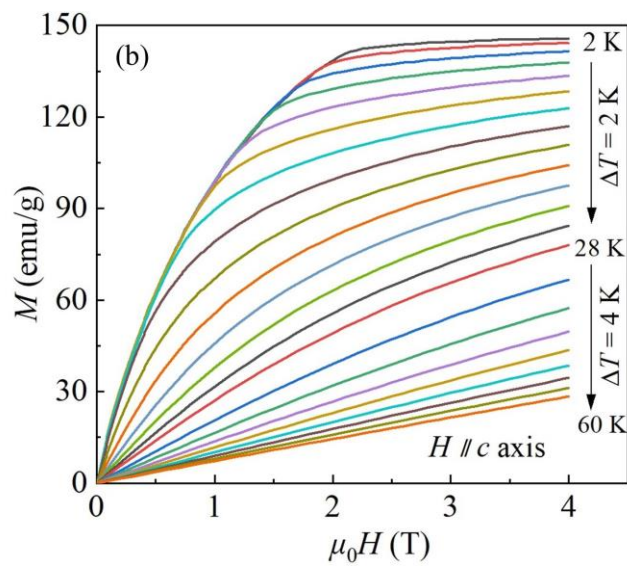
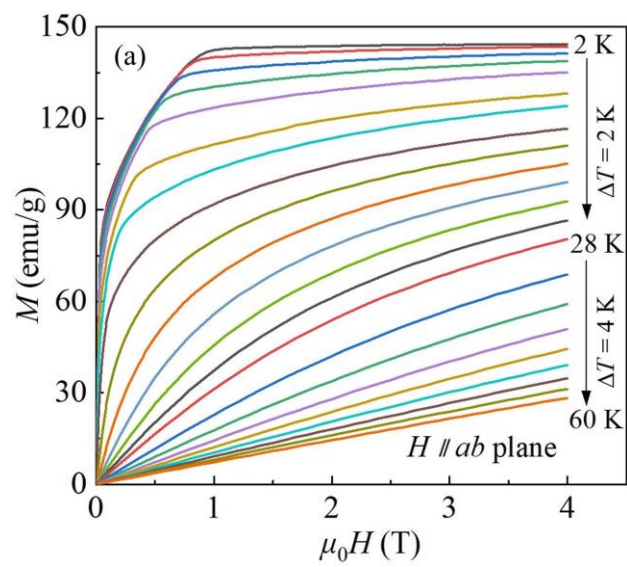


FIG. 4

